Combined effects of crystallography, heat treatment and surface polishing on blistering in tungsten exposed to high-flux deuterium plasma

Y. Zayachuk[a, b] *, I. Tanyeli[c], S. Van Boxel[b], K. Bystrov[c] T. W. Morgan[c], and S.G. Roberts[a, b]

[a]Department of Materials, University of Oxford, Parks Road, Oxford OX1 3PH, UK
[b]Culham Centre for Fusion Energy, Culham Science Centre, Abingdon OX14 3DB, UK
[c]FOM Institute DIFFER, Trilateral Euregio Cluster, De Zaale 20, 5612 AJ Eindhoven, Netherlands

Abstract: for tungsten exposed to low-energy hydrogen-plasmas, it has been thought that grains with <111> surface normal are most susceptible to blistering while those with <001> surface normal are virtually impervious to it. Here, we report results showing that non-uniformity of blister distribution depends on the state of the surface due to polishing. In electrochemically polished material blisters appear on the grains with all orientations, while in mechanically polished material blister-free areas associated with particular orientations emerge. On the other hand, blistering is shown to have a strong dependence on the level of deformation within particular grains in partially recrystallized material.

Keywords: tungsten, plasma exposure, deuterium plasma, blistering, orientation

1. Introduction

Tungsten is one of the main candidate plasma-facing materials for future fusion reactors. Exposure of tungsten to plasma with a high ion flux of hydrogen isotopes under conditions comparable to those at the plasma-wall boundary in a fusion reactor leads to the formation of macroscopic sub-surface cavities, associated with surface blistering [1][2]. An often-reported feature of the blistering process is its non-uniformity – micrographs of the plasma-exposed surfaces reveal regions of intense blistering directly neighbouring blister-free regions [3][4]. Orientation imaging using electron backscatter diffraction (EBSD) indicates that these regions of different blistering characteristics correspond to different grains separated by high-angle grain boundaries [5].

This orientation dependence of blistering has been viewed as an intrinsic property of tungsten and has led to the suggestion of the possibility of tailoring the plasma-facing components in such a way as to avoid the grains with blister-prone orientations (those with surface normals close to <111>) and increasing the size and number of grains with blister-free orientations (those with surface normals close to <001>) [5].

In this paper we present observations of blistering patterns on plasma-exposed tungsten where the distribution of blisters does not follow the commonly accepted view. Blisters appear over the entire surface, with no blister-free regions observed, even where the crystallographic orientation suggests that blisters should be absent, or at least strongly suppressed.

2. Experiment

A tungsten sample was sliced out of a 99.95% purity, 20 mm diameter tungsten rod procured from Goodfellow Metals (UK). It was heat treated in vacuum (~10^{-5} mBar) at 1700 K for 20 hours. Fig. 1 presents the EBSD misorientation map of the typical microstructure produced by such a treatment. In this mode, for each grain an average orientation is calculated, than at each location within this grain a value of misorientation between its orientation and the average value is calculated and assigned a colour code. It demonstrates that material is partially recrystallized (grains with low, below ~1.5°, internal misorientation are recrystallized, others are still deformed).This is similar to the results reported in [6]. The sample's surface was electrochemically polished using 0.5 wt.% aqueous NaOH solution at a voltage of 10 V.

Plasma exposure was performed in the linear plasma generator Pilot-PSI (FOM Institute DIFFER, Netherlands [7]). In this device the plasma is generated by a cascaded arc discharge. Radial electron temperature and density profiles (and therefore also particle and heat flux profiles) within the plasma beam are approximately Gaussian with a FWHM of ~10 mm. The ion flux arriving at the surface of the specimen is calculated from the electron temperature and density measured by Thomson scattering as in [8]. The surface temperature of a specimen is monitored by an IR camera. The sample was exposed to a ~50 eV (energy determined by sample bias and ion temperature) deuterium ion fluence of 10^{27} m^{-2} at an ion flux of 1.1×10^{24} m^{-2}s^{-1}, and at a surface temperature of 650 K; values of both flux and temperature given are maximum values, i.e. those in the center of the plasma beam.

Surface blistering was investigated after plasma exposure using scanning electron microscopy (SEM) and focussed ion beam (FIB) cross-sectioning, both performed using a dual beam FEG Zeiss Auriga FIB-SEM. The interconnection between observed surface and subsurface features and local crystallographic structure was

established using electron backscatter diffraction (EBSD) carried out on a Zeiss EVO scanning electron microscope equipped with a Brucker Quantax EBSD detector.

3. Results and discussion

Fig. 2a shows the typical appearance of the surface after the plasma exposure. A notable feature of the observed blistering pattern is the absence of blister-free areas. In the light of the usual interpretation of blistering dynamics – that there are grain orientations promoting blistering and those suppressing it – this could be explained by simply assuming that all the visible grains have blistering-promoting orientations. However, Fig. 2b presents an EBSD map of surface normal orientations overlaid over the same area, and it is evident that a range of orientations is present, and in particular a grain with <001> surface normal. Such grains usually are reported to be blister-free; however, in this example – and similarly on other near-<001> oriented grains – this is not the case.

There is a different kind of local non-uniformity observed here, however. Two different types of blistering pattern are observed. Some areas (denoted as Type 1 in Fig. 2a) feature dense populations of small blisters (areal density $\sim 3.5 \times 10^5$ mm^{-2}, ~ 0.4–1.5 µm diameter), while other areas (denoted as Type 2) feature relatively sparse populations of large blisters ($\sim 8.8 \times 10^4$ mm^{-2}, $\sim 1.5 - 6$ µm diameter). Fig. 3 presents the close-ups of the corresponding areas, and Fig. 4 presents their FIB cross-sections. The small Type 1 blisters are associated with sub-surface cavities located very close to the surface, whereas Type 2 blisters correspond to large cavities located much deeper below the surface. However, the distribution of the two blister types is not related to the grain orientation. For example, the areas denoted as X and Y in Fig. 2 are two grains with close surface normal orientations, but featuring different blistering patterns.

Fig. 2c shows a misorientation map of the area under consideration. The areas of Type 1 and Type 2 blistering correspond to regions within grains with high and low values of internal misorientation respectively. Thus it can be surmised that in this partially recrystallized material, grains retaining some work-hardening, with high internal misorientation, tend to form deuterium-filled gas bubbles close to the surface and with multiple nucleation centres, whereas fully recrystallized grains tend to form bubbles deeper beneath the surface and with a lower number of nucleation centres.

This difference can be rationalized if it is assumed that nucleation sites are associated with dislocations (as was suggested in [9]). Thus, in the more deformed regions with higher dislocation density:
a) bubble nucleation will tend to occur closer to the surface as there are more potential sites available, increasing the probability of incoming deuterium being trapped;
b) since there are more bubbles formed while the amount of implanted and diffusing deuterium is the same (as it is determined by the exposure flux), each individual cavity will contain less deuterium and will be smaller in size.

A major difference between the experiments described here and those previously reported ([3] [4][5]) is in the surface treatment of the samples. Here electrochemically polished samples were used, leading to a deformation-free surface. The earlier studies of local non-uniformity of blistering did not use electropolished surfaces, with surface preparation being by mechanical polishing only, producing some degree of near-surface deformation. This then implies that the orientation-dependence of blistering appears only if sufficient near-surface deformation is present over all grains. Bubble distribution therefore is not purely an intrinsic crystallographically-dependent property of the material but rather depends on the surface preparation of samples used for the investigation of blistering.

In order to study this behaviour further, a set of samples with different surface conditions was prepared from the same material batch. Sample W1 was ground using 2500 grit SiC abrasive paper. Sample W2 was ground as W1, and additionally polished with 3 µm diamond suspension. Sample W3 was treated as W2, and additionally polished with 0.05 µm colloidal silica suspension. Finally, sample W4 was treated as W3, and then electrochemically polished as described earlier. Following the surface preparation step, all samples were annealed in vacuum at 1300 K for 1 hour.

All the samples from this set were exposed to identical plasma conditions, with a maximum deuterium ion flux of 8×10^{23} m^{-2}s^{-1}, time duration of 70 s, ion fluence (calculated in the location of maximum ion flux) of $\sim 5 \times 10^{25}$ m^{-2}, maximum surface temperature of ~ 450 K and ion energy of ~ 50 eV.

Fig. 5 compares typical blistering patterns observed on the surfaces of samples W3 (mechanically polished with colloidal silica) and W4 (electropolished). A fundamental difference in the character of the distribution of blisters is evident – the mechanically polished sample features blister-free areas whereas the electropolished sample is completely covered with blisters (although it can be seen that exact shapes and densities of blisters on different grains are somewhat different). In the mechanically polished sample the blister-free grains are the ones with surface normal close to <001>, as previously found.

It should be noted that on the rougher mechanically polished surfaces blisters might be more difficult to visually detect. Therefore, to ascertain the absence of blisters the images of FIB cross-sections were used as well. Fig. 6 compares such cross-sections normal to the surfaces of samples W3 and W4. In both cases the cross-section runs across a boundary between grains with <111> and <001> surface normals. In the mechanically

polished sample W, only the grain with <111> surface normal features subsurface cavities, confirming the results of surface imaging, while in the electropolished sample W4, subsurface cavities can be observed in both grains.

Comparing the samples polished to different degrees, there is a trend for the blistering to be suppressed when quality of polishing decreases. Importantly, dynamics of this suppression as a function of the surface state is different for grains with different orientations. Blisters on the grains with <111> surface normal are the most resilient – they appear on the surfaces of all the samples, with the exception of the W1 sample, where no blisters are observed at all. Blisters on the grains with <001> surface normal are present on electropolished surfaces but not on any surfaces polished only mechanically, even one polished with colloidal silica (sample W3). For grains with intermediate orientations, such as <101>, as the number of polishing steps increases, the blisters gradually become more prominent, as illustrated in Fig. 7. This explains the difference in distribution of blisters on the surface of samples polished differently, as shown in Fig. 5 – at electropolished surfaces all grains feature blisters, while at mechanically polished ones on certain grains blistering is suppressed while on others it's not, giving rise to the observed grain dependence. Ultimately, when surface is sufficiently rough, blisters are absent everywhere.

Observations of this suppression also seem to offer a plausible explanation of why blisters are normally not observed in the tokamak experiments, i.e. on actual plasma-facing components (PFCs) exposed to relevant plasma conditions in fusion devices [10]: their surfaces are typically not polished, and as has been demonstrated here (as well as in the previous reports, such as [11]) surface roughness suppresses blistering.

It is not entirely clear what is the mechanism of the suppression of near-surface blistering on the rough surfaces. It can be suggested that it is due to the presence of fast diffusion channels connected to the surface, leading to the reduction of the near-surface deuterium concentration and thus the reduction of driving force for the formation of cavities. Such channels may be provided by a continuous dense dislocation network, or by the microcracks, both of which are more likely to be present on the surfaces deformed by the mechanical surface treatment.

The observed dependence of blistering – or taken broadly, plasma-induced modification – on residual near-surface deformation (seen here as internal misorientation) in partially recrystallized tungsten may be important from the point of view of possible local recrystallization during local transient heat loads and off-normal events ([12][13][14]). These results indicate that the dynamics of plasma-induced modification and associated hydrogen isotope retention is more complex and more non-linear than previously assumed ([15][16]). Deuterium accumulation and blistering might suppress near-surface thermal transport [17] enhancing material modification due to thermal transients [18]. Consequently, blistering behaviour is dynamically non-uniform – locally changing due to the thermal effects, and in turn leading to the changes of material's response to the thermal effects. This should be taken into account when making predictions of hydrogen isotope accumulation in, and ultimately lifetime of, plasma-facing components.

4. Conclusions

A study of the dependence of blistering on the surface of tungsten exposed to divertor-relevant high-flux ($\sim 10^{24}$ m^{-2}s^{-1}) low-energy (~ 50 eV) deuterium plasma on state of the surface due to polishing, heat treatment and local crystallographic structure has been performed.

It is found that the non-uniformity of plasma-induced blistering due to crystallographic orientation, while present to certain extent, is not sufficiently strong as to render certain orientations intrinsically impervious to blistering, manifesting itself only in the differences in blister shape and density. The occurrence of non-uniform blistering patterns where blistered areas neighbour the blister-free ones depends on the degree of mechanical polishing. It is not observed in the case of electrochemically polished samples, i.e. in the absence of a surface-damaged layer – such samples feature blisters on all grains. It is observed that when mechanical polishing is introduced, blistering in general is suppressed. For a given degree of polishing the level of suppression depends on the orientation, with grains with <111> surface normal being the most resilient and grains with <001> surface normal becoming blister-free even after small amounts of mechanical polishing. Because of this, mechanically polished samples feature blistered areas alongside with blister-free ones, depending on orientation.

It is also found that size and density of blisters depends on the annealing state of the individual grains in heat-treated tungsten. Recrystallized grains tend to feature low densities of large blisters corresponding to the cavities located deep in the material, while deformed grains feature high densities of small blisters caused by the near-surface cavities.

Acknowledgements

References

[1] M. Y. Ye, H. Kanehara, S. Fukuta, N. Ohno, and S. Takamura, JNM 313 (2003) 72–76.

[2] M. Balden, S. Lindig, A. Manhard, JNM 414 (2011) 69–72.

[3] W. M. Shu, A. Kawasuso, T. Yamanishi, JNM 386 (2009) 356–359.

[4] R. D. Kolasinski, M. Shimada, Y. Oya, D. A. Buchenauer, T. Chikada, D. F. Cowgill, D. C. Donovan, R. W. Friddle, K. Michibayashi, and M. Sato, J. Appl. Phys. 118 (2015) 073301.

[5] W. M. Shu, A. Kawasuso, Y. Miwa, E. Wakai, G.-N. Luo and T. Yamanishi, Phys. Scr. T128 (2007) 96–99.

[6] A. Manhard, K. Schmid, M. Balden, and W. Jacob, JNM 415 (2011) S632–S635

[7] G. J. van Rooij, V. P. Veremiyenko, W. J. Goedheer, B. de Groot, A. W. Kleyn, P. H. M. Smeets, T. W. Versloot, D. G. Whyte, R. Engeln, D. C. Schram, and N. J. Lopes Cardozo, Applied Physics Letters 90 (2007) 121501.

[8] H. J. van der Meiden, R. S. Al, C. J. Barth, A. J. H. Donné, R. Engeln, W. J. Goedheer, B. de Groot, A. W. Kleyn,W. R. Koppers, N. J. Lopes Cardozo, M. J. van de Pol, P. R. Prins, D. C. Schram, A. E. Shumack, P. H. M. Smeets, W. A. J. Vijvers, J. Westerhout, G. M. Wright, and G. J. van Rooij, Review of Scientific Instruments 79 (2008) 013505.

[9] D. Terentyev, V. Dubinko, A. Bakaev, Y. Zayachuk, W. Van Renterghem and P. Grigorev, Nucl. Fusion 54 (2014) 042004.

[10] M. Balden, V. Rohde, S. Lindig, A. Manhard, K. Krieger, ASDEX Upgrade Team, JNM 438 (2013) S220–S223.

[11] D. Nishijima, H. Iwakiri, K. Amano, M.Y. Ye, N. Ohno, K. Tokunaga, N. Yoshida and S. Takamura, Nucl. Fusion 45 (2005) 669–674.

[12] N. Farid, S. Harilal, O. El-Atwani, H. Ding, and A. Hassanein, Nucl. Fusion 54 (2014) 012002.

[13] A. Suslova, O. El-Atwani, D. Sagapuram, S. S. Harilal and A. Hassanein, et al, Sci. Rep. 4 (2014) 6845.

[14] Y. Igitkhanov and B. Bazylev, Phys. Scr. T145 (2011) 014056.

[15] D. Nishijima, Y. Kikuchi, M. Nakatsuka, M. J. Baldwin, R. P. Doerner, M Nagata and Y Ueda, Phys. Scr. T145 (2011) 014053.

[16] Y. Zayachuk, M.H.J. 't Hoen, P.A. Zeijlmans van Emmichoven, I. Uytdenhouwen and G. van Oost, Nucl. Fusion 52 (2012) 103021.

[17] K.R. Umstadter, R. Doerner and G.R. Tynan, Nucl. Fusion 51 (2011) 053014.

[18] T.W. Morgan, J. J. Zielinski, B. J. Hensen, H. Y. Xu, L. Marot, G. De Temmerman, JNM 438 (2013) S784–S787.
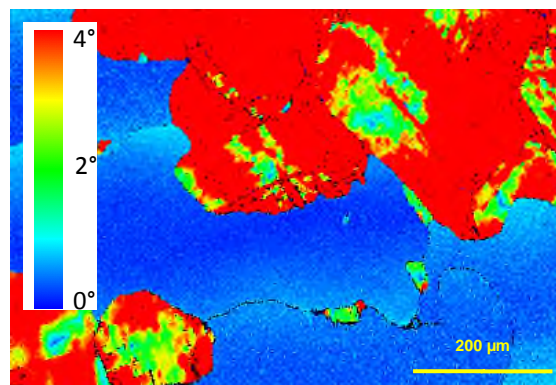
Fig. 1. Typical microstructure of heat-treated tungsten: misorientation map.
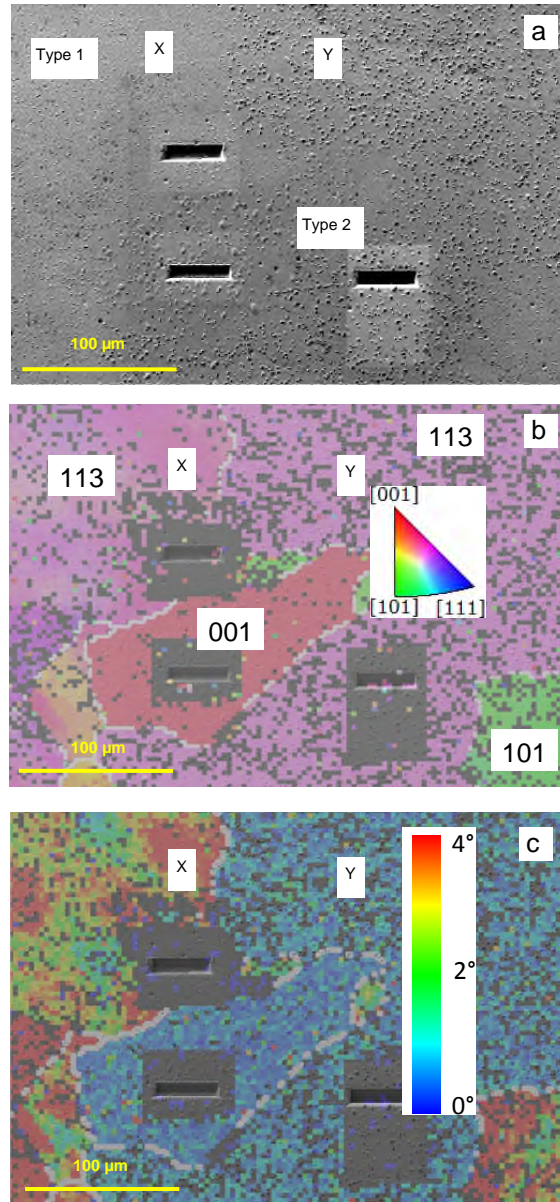
Fig. 2 (a) Surface SEM image of a typical appearance of the plasma-exposed surface (the black rectangles are sites of FIB cross-sections); (b) same image superimposed with EBSD orientation map; (c) same image superimposed with misorientation map. Light grey lines denote high-angle grain boundaries. Orientation and misorientation colour codes are shown.
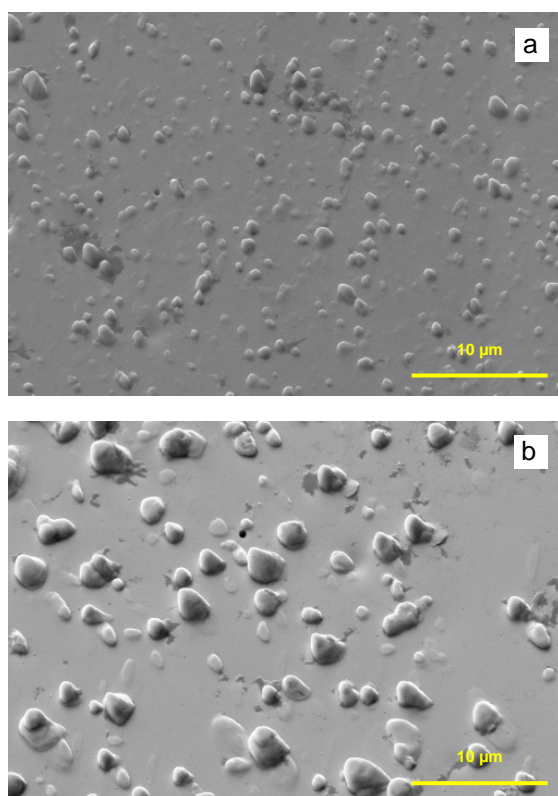
Fig. 3 High-magnification images of blisters: (a) Type 1, (b) Type 2. Magnification is the same in both images.

Fig. 4 Subsurface structures associated with (a) Type 1 and (b) Type 2 blisters (indicated by arrows).
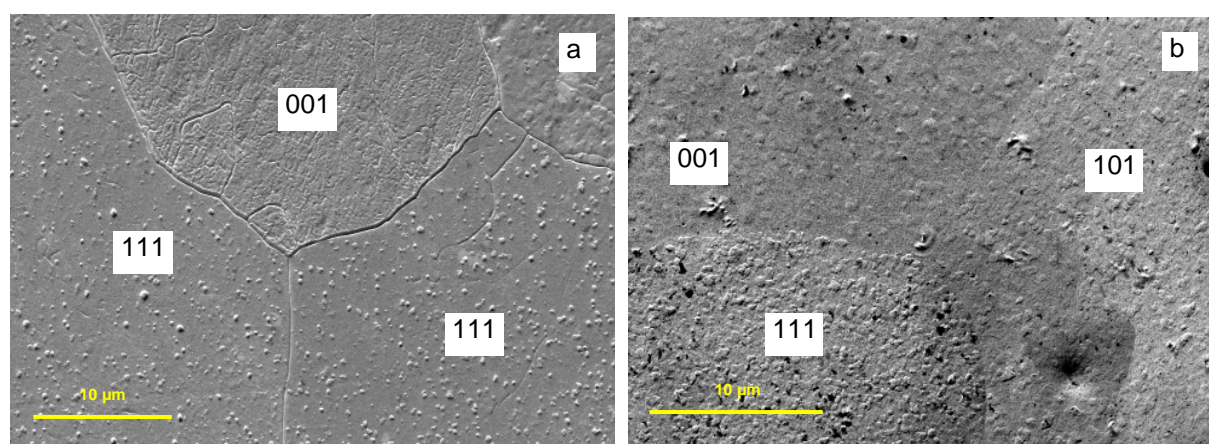
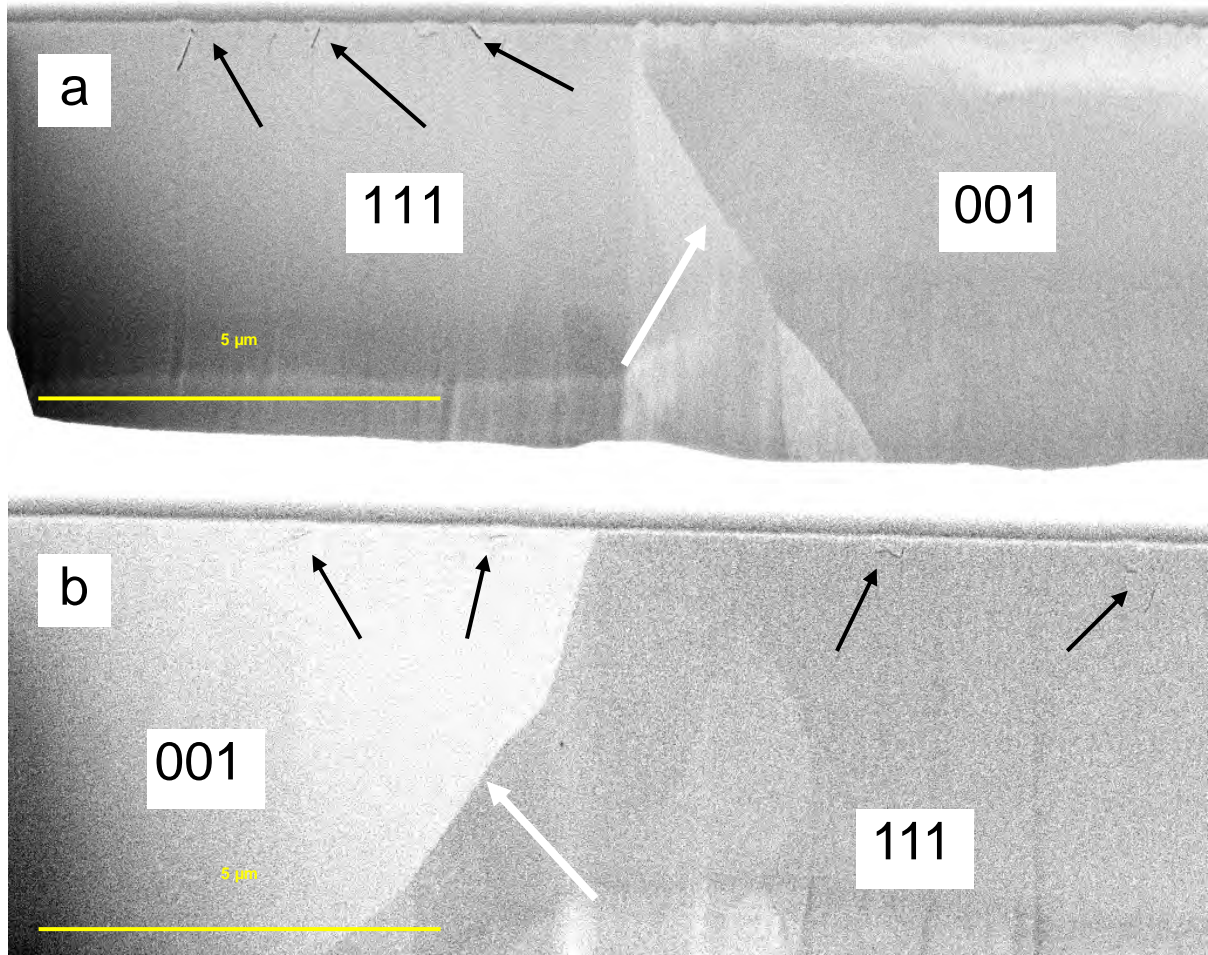Fig. 5 Typical blistering patterns on samples (a) W3 and (b) W4.

Fig. 6 FIB cross-sections of the area near a boundary between grains with <001> and <111> surface normals; (a) sample W3, (b) sample W4. The grain boundary is denoted by white arrow, subsurface cavities by black arrows.

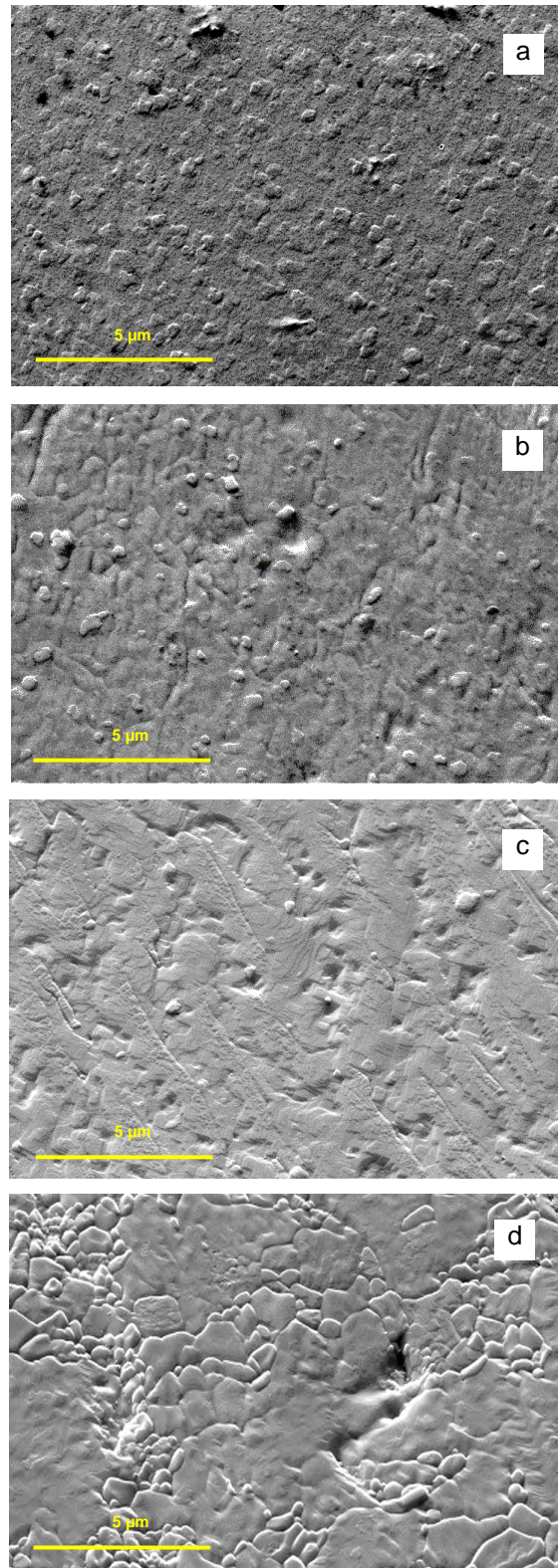Fig. 7 Typical appearance of the surface structure of a grain with <101> surface normal; samples (a) W4, (b) W3, (c) W2, (d) W1.